

Ceramic/natural rubber composites: influence types of rubber and ceramic materials on curing, mechanical, morphological, and dielectric properties

Subhan Salaeh · Nantakan Muensit ·
Pornsuda Bomlai · Charoen Nakason

Received: 28 July 2010/Accepted: 6 October 2010/Published online: 21 October 2010
© Springer Science+Business Media, LLC 2010

Abstract Influence of different types of rubber and ceramic material on cure characteristics, mechanical, morphological, and dielectric properties of natural rubber (NR) vulcanizate was studied. Two types of ferroelectric ceramic materials: barium titanate (BaTiO_3) and lead titanate (PbTiO_3) were prepared by solid-state reaction with calcinations at 1100 °C for 2 h. The ceramic powders were then characterized by X-ray diffraction (XRD), particle size analyzer, and SEM techniques. Ceramic/rubber composites were then prepared by melt mixing of rubber and ceramic powders. Two different types of NR (i.e., epoxidized NR [ENR] and unmodified NR) and two types of ceramic powders (i.e., BaTiO_3 and PbTiO_3) were exploited. It was found that incorporation of ceramic powders in rubber matrix and the presence of epoxirane rings in ENR molecules caused faster curing reaction, and higher delta torque but lower elongation at break. This is attributed to lower mobility of molecular chains and higher interaction between ENR molecules. Furthermore, SEM results revealed that the BaTiO_3 composites showed finer and better distribution of the particles in the rubber matrix than that of the PbTiO_3 composite. This caused superior mechanical properties of the BaTiO_3 composites. Furthermore, higher dielectric constant and loss tangent was observed in the ENR/ BaTiO_3 composites.

Introduction

Ceramic materials based on perovskite-like oxide structures have been currently interested in electrical and electronic applications. Barium titanate (BaTiO_3) and lead titanate (PbTiO_3) are such materials that exhibit high dielectric constant and piezoelectric properties with the Curie temperature (T_c) of approximately 120 and 490 °C, respectively. These two types of materials have been used in various applications: multi-layer ceramics capacitors (MLCC), piezoelectric sensors, transducers, actuators, and microelectromechanical systems (MEMS) [1–3]. Ferroelectric ceramics typically exhibit excellent thermal stability and functional properties of dielectric and piezoelectric properties with high stiffness and low toughness. Therefore, combination of high piezoelectricity of ferroelectric ceramic with high viscoelastic elastomer to form flexible ferroelectric composites has been one of the interested areas in recent years [4]. The desired characteristics of these materials are hybrid properties of the composites with high dielectric constant and stiffness of ceramic materials and excellent mechanical strength, flexibility, formability, and robustness of polymer. General properties of ceramic/polymer composites depend on intrinsic properties of the ceramic and polymer, volume fraction, connectivity, and polarizability of the ceramic particles and polymer matrix. Therefore, ferroelectric composites based on ceramic particles and polymer matrices have been currently developed to embed in the electrical devices [5–7]. Various advantages of these materials are high dielectric constant, lightweight, high mechanical strength, and good flexibility.

The composites with active piezoelectric ceramic particles (0-D) dispersed in three-dimensionally connected polymer matrix (3D) are referred to as 0-3 connectivity [8].

S. Salaeh · C. Nakason (✉)
Center of Excellence in Natural Rubber Technology (CoE-NR),
Prince of Songkla University, Pattani, Thailand
e-mail: ncharoen@bunga.pn.psu.ac.th

N. Muensit · P. Bomlai
Faculty of Science, Prince of Songkla University,
Songkhla, Thailand

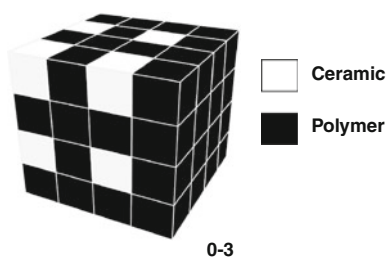


Fig. 1 0-3 Connectivity model in a diphasic composite system

That is, the ceramic particles do not contact to each others but the polymer phase is self-connected in all directions in the 0-3 connectivity, as schematically shown in Fig. 1. Examples of the composites with 0-3 connectivity include lead zirconate titanate (PZT)/polyvinylidene fluoride (PVDF) [9], lead titanate (PT)/polyvinylidene fluoride-trifluoroethylene (PVDF-TrFE) [10], lithium tantalum oxide (LT)/PVDF-TrFE [5], and barium titanate (BT)/PVDF-TrFE [6]. The polymer matrix based on PVDF and its copolymer has been widely used in recent years owing to their intrinsic ferroelectricity. Furthermore, other types of the polymeric matrices have been used. These include polyurethane [11], polyimide [12, 13], polystyrene [14], and epoxy [15]. Moreover, various types of elastomeric matrices have also been applied to prepare the composites. These include silicone rubber (Q) [16], chloroprene rubber (CR) [17], and acrylonitrile butadiene rubber (NBR) [18]. It was claimed that these types of elastomer could be used to prepare the composite materials with the piezoelectric and pyroelectric properties. The composite of natural rubber (NR) may provide the material with good mechanical properties, high flexibility, and superior elasticity. However, NR exhibits intrinsically poor electrical properties with low dielectric constant ($\epsilon' = 2.68$ at 1 kHz) [19], compared with the PVDF ($\epsilon' = 12$ at 1 kHz) [20]. Therefore, modified form of NR by incorporation of polar functional groups (such as epoxidized NR, ENR, as shown in Fig. 2) might cause improving of electrical properties of the composites.

In this work, ENR was used as a polymeric matrix to prepare 0-3 connectivity composites with barium titanate

and lead titanate. Unmodified NR in the form of air-dried sheet (ADS) was also used to prepare the composites for a comparison purpose. Curing, mechanical, morphological, and dielectric properties of the ceramic/NR composites were investigated.

Experimental

Materials

Natural rubber (NR) (air-dried sheet, ADS) was manufactured by Khuan Pun Tae Farmer Co-operation (Phattaluang, Thailand). ENR with 25 and 50 mol% epoxide (i.e., Epoxyprene 25 (ENR-25) and Epoxyprene 50 (ENR-50)) were manufactured by Muang Mai Guthrie Public Co., Ltd. (Suratthani, Thailand). The zinc oxide (white seal) and stearic acid used as activators in sulfur vulcanization system were manufactured by Metoxide Thailand Co., Ltd. (Pathumthani, Thailand) and Imperial Industry Chemical Co., Ltd. (Pathumthani, Thailand), respectively. Mercaptobenzothiazole (MBT) used as an accelerator was manufactured by Flexsys (Termoli, Italy). The sulfur used as curing agent was manufactured by Ajax Chemical Co., Ltd. (Samutprakarn, Thailand). The barium carbonate (BaCO_3), lead oxide (PbO), and titanium dioxide (TiO_2) used as reactants for synthesizing of barium titanate and lead titanate were manufactured by Ajax Finechem Pty Ltd. (New South Wales, Australia), Sigma-Aldrich Pte Ltd. (Buchs, Switzerland) and Sigma-Aldrich Pte Ltd. (St. Louis, USA), respectively. Isopropanol (commercial grade) was used as solvent medium in ball-milling process was manufactured by Shell Chemicals (Thailand) Co., Ltd. (Rayong, Thailand). High purified silver paint was used to cover the surface of the composite sheet for electrical measurement was manufactured by SPI supplies (West Chester, PA, USA).

Preparation of BaTiO_3 and PbTiO_3

Barium titanate (BaTiO_3) and lead titanate (PbTiO_3) were synthesized by the conventional solid state reactions of $\text{BaCO}_3\text{TiO}_2$, and PbOTiO_2 , respectively. Starting materials (i.e., $\text{BaCO}_3\text{TiO}_2$, and PbOTiO_2) were first weighed with a molar ratio of 1:1. They were then incorporated into a 1-L ball-milled jar and thoroughly mixed for 1 min. Isopropanol was then added until 75 vol% of the jar was reached. The mixing was continued for 5 min. The mixture was then ball milling for another 24 h using zirconia balls with a half capacity of the jar. Isopropanol was thereafter separated by rotary evaporator. The remaining product was then dried at 120 °C for 12 h in a hot air oven. The mixed powder was then grinded, sieved through 120 mesh screen, and then incorporated into the alumina crucible.

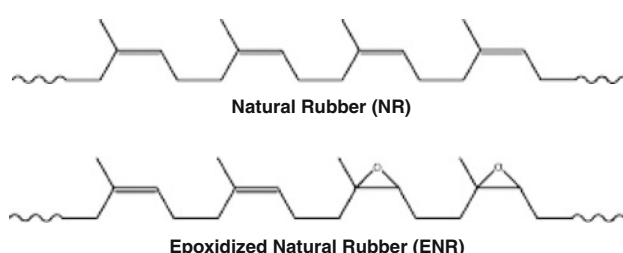


Fig. 2 Molecular structures of natural rubber and epoxidized natural rubber

Calcination was then performed at 1100 °C for 2 h in the muffle furnace (Thermolyne 6000 furnace, Barnstead International, Dubuque, IA, USA).

Preparation of ceramic/NR composites

BaTiO_3/NR and PaTiO_3/NR composites were prepared by mixing process at 60 °C using an internal mixer with a capacity of 80 cm³, (Brabender Plasticorder, model PLE331, Brabender OHG Duisburg, Germany) at a rotor speed of 60 rpm. Two different types of NR were used: unmodified NR (i.e., ADS) and ENR with two different levels of epoxide groups (i.e., 25 mol% (ENR-25) and 50 mol% (ENR-50)). Compounding formulation used to prepare the composites and mixing schedule are shown in Table 1. NR was first masticated for 5 min. Zinc oxide and stearic acid were then added and mixed for 2 and 1 min, respectively. Ceramic powders were then incorporated into the chamber and continued mixing for another 5 min. After dumped the mixes out of the mixing chamber, MBT and sulfur were added and mixed using two-roll mill for 1 and 2 min, respectively. The rubber compound was then sheeted out and left at room temperature for 12 h before testing and vulcanizing.

XRD analysis

X-ray diffractometer (XRD) (model X'Pert MPD, Philips, Almelo, The Netherland) with nickel filtered Cu K_α radiation was used to characterize phase structure of BaTiO_3 , PaTiO_3 , and starting materials (i.e., $\text{BaCO}_3/\text{TiO}_2$ and PbO/TiO_2). The 2θ scanning of X-ray intensity in a range of 20–60° with a scan speed of 0.05%/s was used.

Cure characterization

Rotorless rheometer (rheoTECH MD+, Tech Pro, Inc., Cuyahoga Falls, USA) was used to determine curing characteristics of the rubber composites at 160 °C with

Table 1 Compounding formulation used to prepare ceramic/NR composites

Ingredients	Quantities (phr)	Mixing schedule (min)
NR/ENRs ^a	100	5
Zinc oxide	6.0	2
Stearic acid	0.5	1
$\text{BaTiO}_3/\text{PbTiO}_3$	0.2 ^b	5
Mercaptobenzothiazole (MBT)	0.5	1
Sulfur	3.5	2

^a ENR-25 and ENR-50

^b Volume fraction

1° arc and 60 min. The optimum cure time (t_{c90}), scorch time (t_{s1}), minimum torque (M_L), maximum torque (M_H), and delta torque ($M_H - M_L$) were determined from the curing curves. The vulcanizates with a thickness of approximately 550 ± 50 μm was then prepared by compression molding at 160 °C according to the respective optimum cure time (t_{c90}). Mechanical, morphological, and dielectric properties of the composite vulcanizates were then investigated.

Mechanical properties

The dumb-bell shaped specimens were prepared from a sheet of the rubber vulcanizates by die cutting according to ASTM die type C. Stress-strain behavior of the vulcanizates were then tested using a universal tensile testing machine (Hounsfeld Tensometer, model H 10KS, Hounsfeld Test Equipment Co., Ltd, Surrey, U.K.) at a speed of 500 mm/min and initial gauge length of 25 mm, according to ASTM D412.

Microstructure studies

Scanning electron microscopy (SEM) (model JSM-6510LA, Jeol Ltd., Akishima, Japan) was used to characterize microstructures of the ceramic powders and the cryogenic fractured surface of the ceramic/NR composites. The samples were coated with a thin layer of gold under vacuum condition before characterization.

Dielectric measurement

Capacitance and loss tangent (i.e., $\tan \delta$) of the ceramic/NR composites were determined in frequency ranges from 75 kHz to 30 MHz at room temperature using a precision LCR meter (Agilent 4285A, Agilent Technologies, Penang, Malaysia). Samples with diameter of approximately 16 mm and thickness of 0.50–0.60 mm were used. Surfaces of the samples were first painted with a thin layer of high-purity silver paint. The dielectric constant (ϵ') was calculated according to the formula [5]:

$$\epsilon' = \frac{Cd}{A\epsilon_0} \quad (1)$$

The loss tangent was then calculated by the following relation:

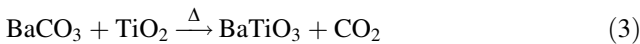
$$\tan \delta = \frac{\epsilon''}{\epsilon'} \quad (2)$$

where C is capacitance (F), ϵ_0 is dielectric constant of free space (8.854×10^{-12} F/m), d is thickness of sample (m), A is the area of electrode (m^2), ϵ' is dielectric constant (the real part), and ϵ'' is loss factor or dielectric loss (the imaginary part).

Results and discussion

XRD analysis

Figure 3 shows XRD patterns of mixed powders BaCO_3 – TiO_2 (Fig. 3a) and calcined product (BaTiO_3) (Fig. 3b). It can be seen that the mixed powders BaCO_3 – TiO_2 exhibited different XRD patterns compared with the BaTiO_3 product. That is, the structure of BaTiO_3 was characterized by XRD peaks at 22.02° , 22.23° , 31.49° , 31.65° , 38.89° , 44.90° , 45.37° , 50.98° , 55.27° , and 56.27° which corresponded to the $(0\ 0\ 1)$, $(1\ 0\ 0)$, $(1\ 0\ 1)$, $(1\ 1\ 0)$, $(1\ 1\ 1)$, $(0\ 0\ 2)$, $(2\ 0\ 0)$, $(2\ 0\ 1)$, $(1\ 1\ 2)$, and $(2\ 1\ 1)$ planes of perovskite structure, respectively [21]. This proves that the reaction of BaCO_3 and TiO_2 at 1100°C yielded BaTiO_3 product, as follows:



XRD patterns of PbTiO_3 and mixed powders of PbO/TiO_2 are shown in Fig. 4. It can be seen that the perovskite

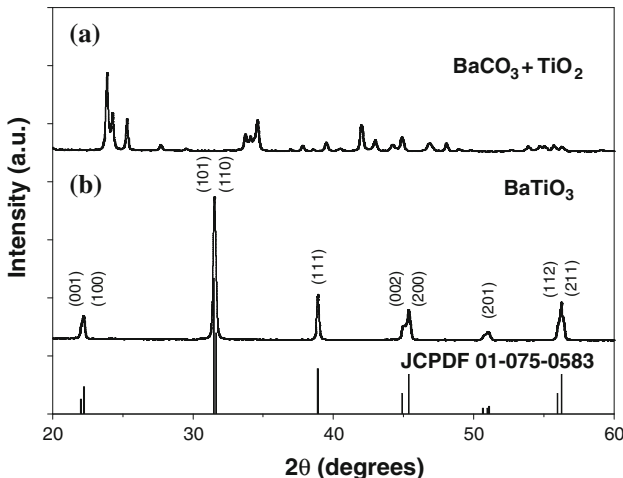


Fig. 3 XRD patterns of (a) BaCO_3 and TiO_2 (b) BaTiO_3

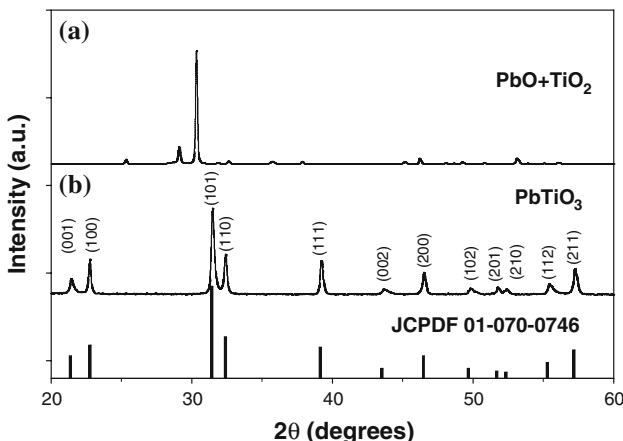


Fig. 4 XRD patterns of (a) PbO and TiO_2 (b) PbTiO_3

structure of PbTiO_3 was also observed. That is, the presence of the peaks at 21.36° , 22.75° , 31.41° , 32.40° , 39.14° , 43.52° , 46.47° , 49.56° , 51.68° , 52.35° , 55.28° , and 57.17° which corresponded to the $(0\ 0\ 1)$, $(1\ 0\ 0)$, $(1\ 0\ 1)$, $(1\ 1\ 0)$, $(1\ 1\ 1)$, $(0\ 0\ 2)$, $(2\ 0\ 0)$, $(2\ 0\ 1)$, $(1\ 1\ 2)$ and $(2\ 1\ 1)$ planes, respectively [22]. Therefore, the reaction of PbO and TiO_2 at 1100°C gave PbTiO_3 product, as shown in Eq. 4. Furthermore, the results in Figs. 3 and 4 agreed with the reported XRD data of the JCPDF files (JCPDF 01-075-0583 and JCPDF 01-070-0746) for BaTiO_3 and PbTiO_3 , respectively [21, 22]. It is noted that the broadness of the observed peaks at 112 and 211 planes related to the size of crystallite of the powder.



It is noted that the broadness of the observed peaks at 112 and 211 planes related to size of crystallite in the powder, which could be estimated by Scherrer equation, as follows:

$$t = K\lambda/(B \cos \theta) \quad (5)$$

where t is the averaged dimension of crystallite, K is the Scherrer constant (0.9), λ is the wavelength of X-ray, B is FWHM (full width at half maximum). High broadening of peak (high B value) resulted in smaller crystallite than that of the narrow peak (low B value).

Cure characteristics

Curing curves of gum and filled rubber compounds (i.e., ceramic/NR composites) are shown in Fig. 5. It can be seen that the plateau curing curves were observed in the gum compound of unmodified NR (i.e., ADS) but reversion phenomenon (i.e., decreasing of torque with increasing

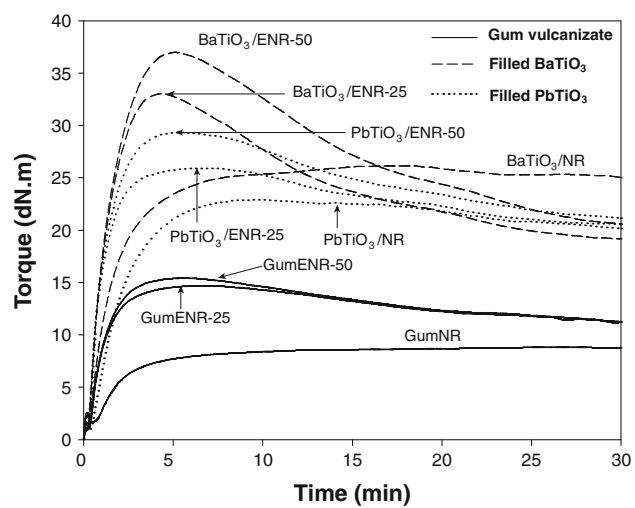


Fig. 5 Curing curves of gum and filled (i.e., ceramic/rubber composites) rubber compound with different types of rubber and ceramic materials

Table 2 Cure characteristics of gum vulcanizates and ceramic/NR composites

Properties	Gum vulcanizates			Filled BaTiO ₃			Filled PbTiO ₃		
	NR	ENR-25	ENR-50	NR	ENR-25	ENR-50	NR	ENR-25	ENR-50
Min. torque (M_L) (dN m)	1.70	1.12	1.37	0.73	1.22	1.32	0.93	1.89	2.06
Max. torque (M_H) (dN m)	8.80	14.69	15.41	26.16	33.04	36.97	22.92	25.94	29.35
Delta torque ($M_H - M_L$) (dN m)	7.11	13.57	14.05	25.43	31.82	35.65	21.99	24.05	27.29
Scorch time (t_{s1}) (min)	1.00	0.43	0.43	0.51	0.31	0.31	0.51	0.34	0.33
Optimum cure time (t_{c90}) (min)	7.00	2.67	2.57	5.19	2.55	3.00	4.71	2.36	2.63
Cure rate index (min ⁻¹)	16.67	44.64	46.73	21.37	44.64	37.17	23.81	49.50	43.48

testing time) was observed in the ENR gum compounds. This is attributed to breakdown of monosulfidic and ether linkages which contributed to the higher reversion in the ENR networks [23]. Higher maximum torque was observed in the ceramic filled rubber compound but the reversion characteristic was more pronounced in particular in the ENR compounds. This is attributed to the restructuring and changing in cross-link structures of the vulcanizates after the maximum vulcanization was achieved [24]. Cure characteristics of the gum rubber compound and the ceramic/NR composites in terms of minimum, maximum and delta torques, scorch time, cure time, and cure rate index (CRI) are summarized in Table 2. It is seen that the ENR compounds with and without ceramic particles showed shorter cure and scorch times but higher cure rate index (CRI) compared with the unmodified NR (i.e., ADS) compounds. This may be attributed to higher reactivity of the double bonds adjacent to the epoxide groups in the ENR molecules [25, 26]. Also, it is clear that incorporation of ceramic particles generated higher frictional heat during mixing process. This caused increasing rate of crosslinking and hence shortening cure time. In the BaTiO₃ composites, longer cure time but lower cure rate index was observed compared with the PbTiO₃ composites. This indicated lower rate of vulcanization in the BaTiO₃ compounds. Furthermore, it can be seen that the delta torque increased with increasing epoxide groups in the ENR molecules. This might be due to higher polarity which led to higher chemical interaction between the rubber molecules and rubber molecules with ceramic particles. Furthermore, incorporation of BaTiO₃ caused higher delta torque than that of the incorporation of PbTiO₃. This may be attributed to higher reinforcing capability of the BaTiO₃ particles in the rubber matrix.

Mechanical properties

Figure 6 shows stress-strain curves of gum and filled vulcanizates (i.e., ceramic/NR composites). It is seen that the ceramic/NR composites exhibited higher Young's modulus (i.e., slope of the linear region of the curves) than

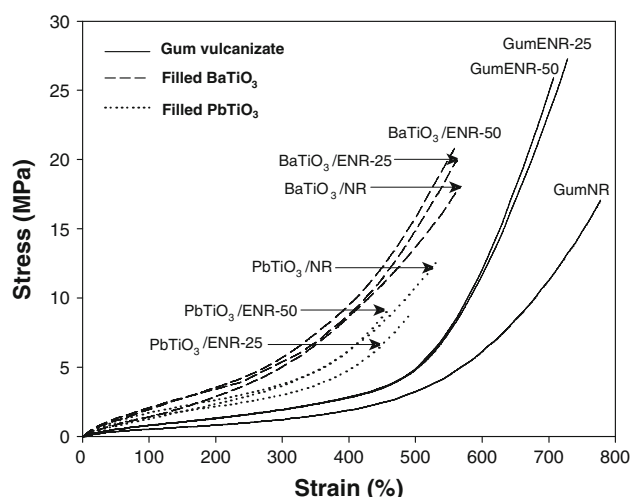


Fig. 6 Stress–strain curves of gum and ceramics/rubber composites vulcanizates with different types of rubber and ceramic materials

those of the gum vulcanizates. This is due to incorporation of the ceramics particles that caused lower mobility of molecular chains and hence increasing stiffness of the materials. This result agreed with increasing delta torque of the composites, as shown in Table 2. In Fig. 6, it is also seen that the gum vulcanize exhibited higher elongation at break than those of the filled ceramic/NR composites. This is attributed to higher chain flexibility of the gum vulcanizates. Mechanical properties in terms of tensile strength and elongation at break based on the failure points of stress–strain curves (Fig. 6) are summarized in Figs. 7 and 8, respectively. It can be seen that the gum and BaTiO₃ filled vulcanizates of ENRs exhibited higher tensile strength but the PbTiO₃ filled vulcanizates showed lower tensile strength than those of the unmodified NR vulcanizates. This may be due to higher chemical interaction between BaTiO₃ particles and ENR matrices which caused higher reinforcing effect. It has been well established that the surface composition of barium titanate consists of hydroxyl groups [27, 28] and metal oxides [29]. Therefore, the existence of chemical interaction and hydrogen bonding between hydroxyl groups and metal oxides with

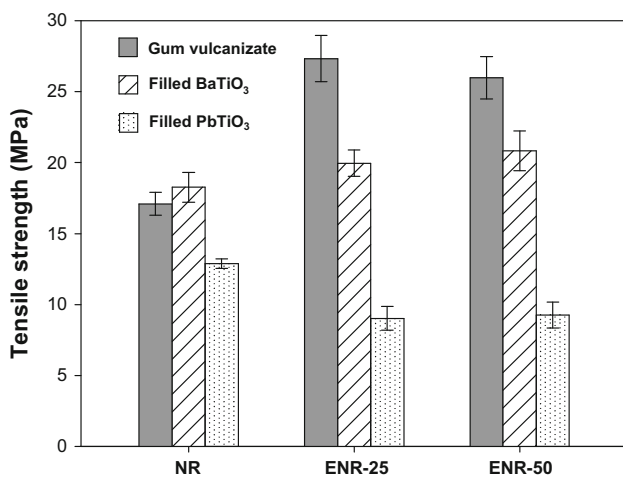


Fig. 7 Tensile strength of gum and ceramics/rubber composites vulcanizates with different types of rubber and ceramic materials

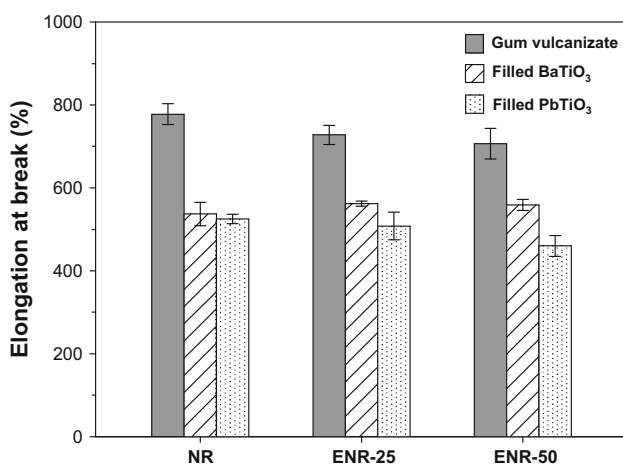


Fig. 8 Elongation at break of gum and ceramics/rubber composites vulcanizates with different types of rubber and ceramic materials

epoxide groups in ENR molecules was pronounced. This might be similar phenomenon to the formation of hydrogen bonding in BaTiO₃/polyimide composites [27]. On the contrary, it was found that mechanical properties of PbTiO₃/ENR composites are lower than those of PbTiO₃/NR materials, and even lower than properties of NR and ENR gum vulcanizates. This might be attributed to larger particles of PbTiO₃ together with poor distribution as large agglomerate in the ENR matrix. In Fig. 8, it is also seen that the unmodified NR vulcanizates exhibited higher elongation at break. This is attributed to lower chemical interaction between ADS molecules. This caused lower restriction of molecular movement during stretching unlike ENR molecules which contain functional groups with higher polarity and hence higher chemical interaction between the chains [30]. In the ceramic/NR composites, it is seen that the BaTiO₃ composites exhibited higher tensile

strength and elongation at break than those of the PbTiO₃ composites. This might be due to better compatibility (i.e., higher chemical interaction) and better distribution of finer BaTiO₃ particles in the rubber matrix. This is a reason why slight increasing of tensile strength of BaTiO₃/ENR vulcanizates was observed with increasing level of epoxide groups. On the other hand, decreasing trend was observed in the PbTiO₃/ENR vulcanizates.

Morphological properties

Figure 9 shows SEM micrographs of BaTiO₃ and PbTiO₃ particles. It can be seen that the BaTiO₃ particles are finer than those of the PbTiO₃ particles. It has been well established that finer particles gave higher surface areas and hence interfacial forces with elastomer [31, 32]. Additional quantitative information of the particle size distributions of BaTiO₃ and PbTiO₃ using laser granulometry experiment is shown in Fig. 10. It is confirmed that the particle size of BaTiO₃ is smaller than that of the PbTiO₃ with the average particle size of approximately 4.55 and 64.74 μm , respectively. Figure 11 shows the cryogenic fractured surfaces of gum and filled vulcanizates (i.e., ceramics/rubber composites). It is seen that the gum vulcanizates exhibited smoother surface compared with the filled vulcanizate (i.e., composites). That is, only white spots of ZnO particles appeared in the images of gum vulcanizates. However, the ceramic particles embedded in the rubber matrix with 0-3 connectivity were clearly observed in the composite materials. It is also seen that the finer particles with better distribution in rubber matrix was observed in the BaTiO₃ composite. Therefore, larger specific surface areas caused higher filler–rubber interaction with the enhancement of mechanical properties. This caused the BaTiO₃ composite exhibited higher Young's modulus (Fig. 6), delta torque (Table 2), and superior mechanical properties (Fig. 7) than those of the PbTiO₃ composites. Furthermore, it is clear that the BaTiO₃ showed the best dispersion in the ENR-50 matrix. This might be attributed to higher level of polar functional groups which caused increasing interaction between BaTiO₃ and ENR-50 matrix. As a consequence, the BaTiO₃/ENR-50 composites exhibited higher tensile strength and Young's modulus than those of the BaTiO₃/ENR-25 and BaTiO₃/unmodified NR composites, respectively. However, the SEM micrographs of the PbTiO₃ composites showed no significant difference among different types of rubber used (i.e., unmodified NR, ENR-25 and ENR-50).

Dielectric properties

Dielectric constant (ϵ') as a function of frequencies in a range from 75 kHz to 30 MHz for gum vulcanizates and

Fig. 9 SEM micrographs of **a** BaTiO₃ and **b** PbTiO₃

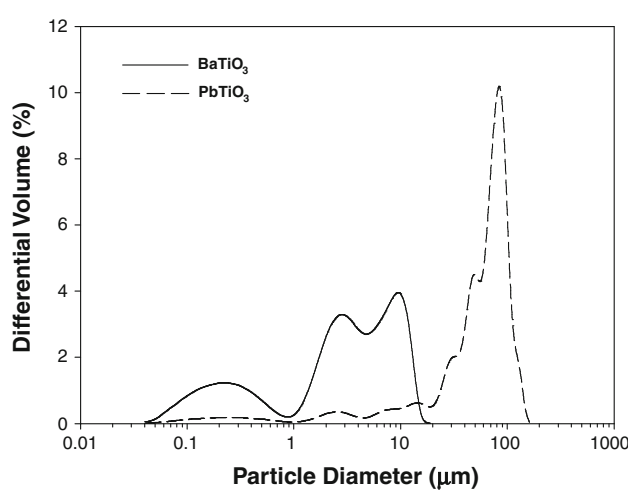
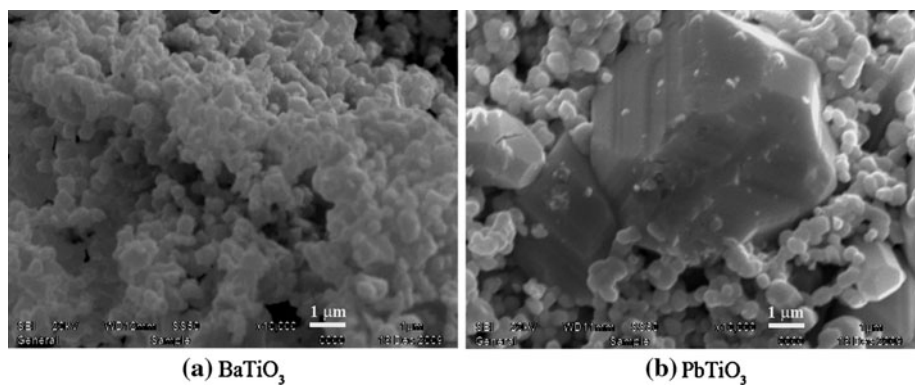


Fig. 10 Particle size distribution of BaTiO₃ and PbTiO₃

composites of BaTiO₃ and PbTiO₃ are shown in Fig. 12. It can be seen that lower dielectric constant was observed in the unmodified gum NR vulcanizates compared with the vulcanizates of composites. Furthermore, the dielectric constant of the unmodified gum NR vulcanizates slight decreased with increasing frequency but abruptly decreasing trend was observed in the ENR gum vulcanizates. This is attributed to orientation polarization where less polar functional groups in polymer chains caused switching field with increasing frequency. As a consequence, decreasing trend of the dielectric constant was observed [12, 33, 34]. In Fig. 12, it is also clear that the abrupt decreasing trend of dielectric constant with increasing frequencies was observed in the ENR composites. This may be attributed to dielectric relaxation of the ceramic particles and the interfaces in the rubber composite [13]. It is also seen that, with a given type of ceramic powder, the dielectric constant of the composite increased with increasing epoxide content in the ENR molecules. This is due to increasing polarity of the rubber phase and hence the dipoles. This led to increasing of orientation polarization and also interfacial polarization [33]. Also, it is seen that incorporation of the

ceramics particles caused increasing of the dielectric constant. This is attributed to interfacial polarization, known as Maxwell–Wagner–Sillar (MWS) effect. This phenomenon appears in the heterogeneous media of different phases with different dielectric constant and conductivity. Therefore, accumulation of charges at the phase boundaries and formation of large dipoles on the ceramic particles or clusters occurred [13, 35]. It is also seen that, at a given frequency, the BaTiO₃ composites exhibited higher dielectric constant than those of the PbTiO₃ composites. This might be due to the intrinsic properties of the BaTiO₃ which typically exhibited higher dielectric constant than that of the PbTiO₃. That is, the dielectric constant of BaTiO₃ and PbTiO₃ are approximately 1700 [36] and 107 [37], respectively.

Figure 13 shows loss tangent as a function of frequencies of gum vulcanizate and composites of BaTiO₃ and PbTiO₃. It is seen that the dielectric relaxation with loss tangent peaks was observed in this frequency ranges. Furthermore, it can be seen that, at a given frequency, the loss tangent increased with the presence and increasing of epoxide groups in the ENR molecules. Furthermore, incorporation of ceramic materials caused increasing of the loss tangent. This could be interpreted by interfacial charge polarization (i.e., Maxwell–Wagner effect) ϵ''_{MW} , intrinsic electric dipole polarization (ϵ''_D) and leakage conductivity loss (ϵ''_{dc}) inside the composite, as described by the following relation [5, 7, 13, 38]:

$$\epsilon'' = \epsilon''_{dc} + \epsilon''_{MW} + \epsilon''_D. \quad (6)$$

The loss tangent is the energy dissipation in the dielectric system. It is proportional to the imaginary part of dielectric constant or loss factor (ϵ''), as shown in Eq. 2. In Fig. 13, it is clear that the ceramic/ENRs composites exhibited lower loss tangent than those of the ENR gum vulcanizates. This result indicated that the ceramic/ENRs composites exhibited higher ability to storage charges or lower energy loss, as compared with the ENR gum vulcanizates. Furthermore, the composites of PbTiO₃/ENR-50 exhibited lower loss tangent than those of the BaTiO₃/ENR-25 composites. This

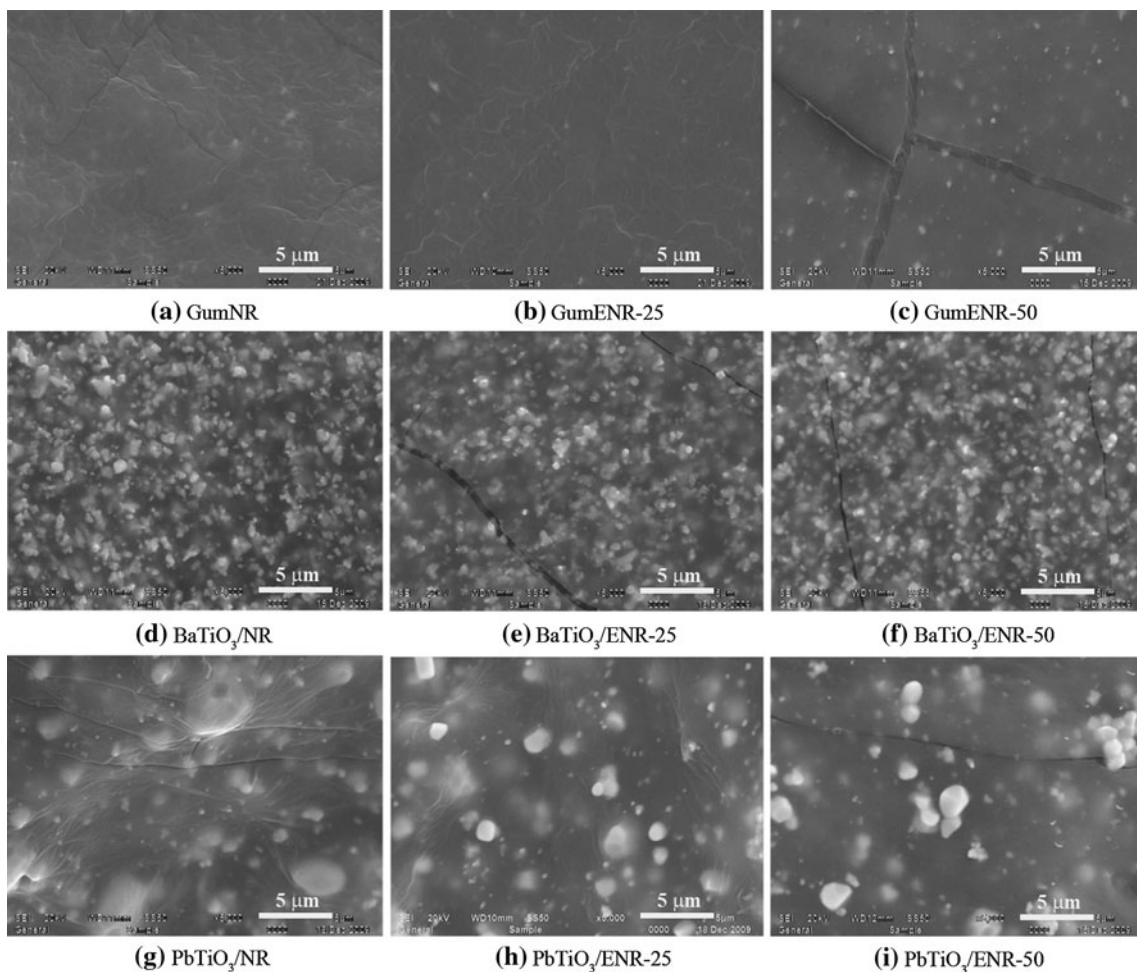


Fig. 11 SEM micrographs of gum filled (ceramics/rubber composites) vulcanizates with different types of rubber and ceramic materials
a NR gum vulcanize; b ENR-25 gum vulcanize; c ENR-50 gum

vulcanizate; d BaTiO₃/NR; e BaTiO₃/ENR-25; f BaTiO₃/ENR-50; g PbTiO₃/NR; h PbTiO₃/ENR-25; i PbTiO₃/ENR-50

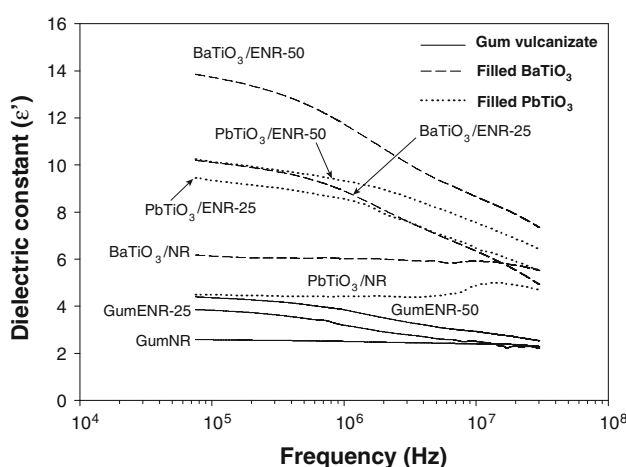


Fig. 12 Dielectric constant (ϵ') as a function of frequency of gum vulcanizates and ceramic/rubber composites with different types of rubber and ceramic materials

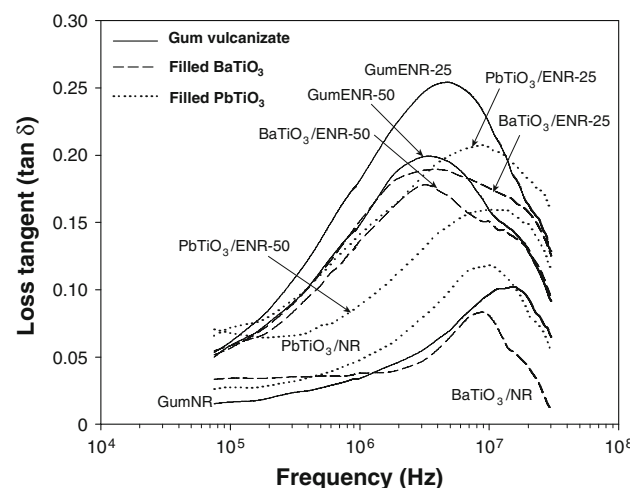


Fig. 13 Loss tangent (tan δ) as a function of frequency of gum vulcanizates and ceramic/rubber composites with different types of rubber and ceramic materials

result proved that the ENR-50 caused higher dielectric constant while retaining excellent loss tangent properties (i.e., lower energy dissipation). However, the PbTiO₃ composites exhibited lower dielectric constant than those of the composites based on BaTiO₃. Therefore, it is concluded that modification by adding polar functional groups in NR molecules together with incorporation of ceramic particles caused enhancement of dielectric constant of NR. This confirms possibility to prepare NR composites with high dielectric constant which could be possible to embed in the electrical devices.

Conclusion

Composites based on blending of different types of rubbers and ceramic materials were prepared. Cure characteristic, mechanical, morphological, and dielectric properties of the ceramic/NR composite were investigated. It was found that the BaTiO₃ and PbTiO₃ were successfully synthesized by the solid-state reaction. X-ray diffraction patterns were used to confirm the perovskite structures of BaTiO₃ and PbTiO₃ after calcination at 1100 °C for 2 h. It was also found that faster scorch time (t_{s1}), cure time (t_{c90}), higher delta torque ($M_H - M_L$) and cure rate index (CRI) were observed in the gum ENR compounds and their composites with ceramic particles. Furthermore, it was found that the gum ENR vulcanizates and BaTiO₃/ENR composites exhibited higher mechanical properties than those of the gum unmodified NR (ADS) vulcanizate and PbTiO₃/ADS. Moreover, the BaTiO₃ composites exhibited finer and better dispersion in the rubber matrix than those the PbTiO₃ composites. An increase in dielectric constant and loss tangent of the ENR gum vulcanizates and ENR composites were also observed. That is, the BaTiO₃/ENR-50 composites exhibited the highest dielectric constant but lower loss tangent.

Acknowledgements The authors gratefully acknowledge the Thailand Research Fund (TRF) through the Royal Golden Jubilee Ph.D. Program (Grant No. PHD/0245/2549). Also, contribution of Prof. Dr. Brahim Elouadi, Université De La Rochelle, La Rochelle, France is acknowledged.

References

- Chen JF, Shen ZG, Liu FT, Liu XL, Yun J (2003) Scripta Mater 49:509
- Kumar P, Singh S, Juneja JK, Prakash C, Raina KK (2009) Physica B 404:1752
- Carter CB, Norton MG (2007) Ceramic materials: Science and engineering. Springer, New York
- Dias CJ, Das-Gupta DK (1996) IEEE Trans Dielectr Electr Insul 3:706
- Guggilla P, Batra AK, Edwards ME (2009) J Mater Sci 44:5469. doi:[10.1007/s10853-009-3753-8](https://doi.org/10.1007/s10853-009-3753-8)
- Li J, Claude J, Norena-Franco LE, Seok SI, Wang Q (2008) Chem Mater 20:6304
- Huang X, Xie L, Jiang P, Wang G, Liu F (2009) J Phys D 42:245407
- Newnham RE, Skinner DP, Cross LE (1978) Mater Res Bull 13:525
- Hilczer B, Kułek J, Markiewicz E, Kosec M, Malič B (2002) J Non-Cryst Solids 305:167
- Ploss B, Ploss B, Shin FG, Chan HLW, Choy CL (2000) IEEE Trans Dielectr Electr Insul 7:517
- Sakamoto WK, Marin-Franch P, Das-Gupta DK (2002) Sens Actuators A 100:165
- Wang SF, Wang YR, Cheng KC, Hsiao YP (2009) Ceram Int 35:265
- Choudhury A (2010) Mater Chem Phys 121:280
- Abraham R, Thomas SP, Kuryan S, Isac J, Varughese KT, Thomas S (2009) Express Polym Lett 3:177
- Wilson SA, Maistros GM, Whatmore RW (2005) J Phys D 38:175
- Safari A, Newnham RE, Cross LE, Schulze WA (1982) Ferroelectrics 41:197
- Banno H (1983) Ferroelectrics 50:3
- Amin M, Osman H, Baloomal L, Darwish KA, Kamal B (1988) Ferroelectrics 81:387
- Nam JD, Choi HR, Koo JC, Lee YK, Kim KJ (2007) In: Kim KJ, Tadokoro S (eds) Electroactive polymers for robotic applications: artificial muscles and sensors. Springer, London
- Das-Gupta DK (1991) Ferroelectrics 118:165
- JCPDF no. 01-075-0583, International centre for diffraction data, 2003
- JCPDF no. 01-070-0746, International centre for diffraction data, 2003
- Poh BT, Kwok CP, Lim GH (1995) Eur Polym J 31:223
- Kruželák J, Kyselá C, Hudec I (2008) KGK-Kaut Gummi Kunst 61:424
- Poh BT, Chen MF, Ding BS (1996) J Appl Polym Sci 60:1569
- Sadequ AM, Ishiaku US, Ismail H, Poh BT (1998) Eur Polym J 34:51
- Dang ZM, Lin YQ, Xu HP, Shi CY, Li ST, Bai J (2008) Adv Funct Mater 18:1509
- Kim P, Doss NM, Tillotson JP, Hotchkiss PJ, Pan MJ, Marder SR, Li J, Calame JP, Perry JW (2009) ACS Nano 3:2581
- Kim P, Jones SC, Hotchkiss PJ, Haddock JN, Kippelen B, Marder SR, Perry JW (2007) Adv Mater 19:1001
- George V, Britto IJ, Sebastian MS (2003) Radiat Phys Chem 66:367
- Fröhlich J, Niedermeier W, Luginsland HD (2005) Composites A 36:449
- Boonstra BB (1982) In: Blow CM, Hepburn C (eds) Rubber technology and manufacture, 2nd edn. Butterworth-Heinemann, London
- Reffae ASA, El Nashar DE, Abd-El-Messieh SL, Abd-El Nour KN (2009) Mater Des 30:3760
- Popielarz R, Chiang CK, Nozaki R, Obrzut J (2001) Macromolecules 34:5910
- Singh V, Kulkarni AR, Rama Mohan TR (2003) J Appl Polym Sci 90:3602
- Lovinger AJ (1983) Science 220:1115
- Xu D, Ren Q, Chu PL, Chow YT, Chan HP, Cheng SY, Chow B, Guo SY, Yang HL (2004) J Mater Sci 39:6577. doi:[10.1023/B:JMSC.0000044898.04904.6c](https://doi.org/10.1023/B:JMSC.0000044898.04904.6c)
- Xie S, Zhu BK, Wei XZ, Xu ZK, Xu YY (2005) Composites A 36:1152